

# Lensless Wiener-Khinchin telescope based on high-order spatial autocorrelation of light field

ZHENTAO LIU<sup>1</sup>, XIA SHEN<sup>1</sup>, HONGLIN LIU<sup>1</sup>, HONG YU<sup>1</sup>, AND SHENSHENG HAN<sup>1\*</sup>

<sup>1</sup>Shanghai Institute of Optics & Fine Mechanics, Chinese Academy of Sciences, Shanghai, 201800, China

\*Corresponding author: sshan@mail.shcnc.ac.cn

Compiled December 18, 2019

With the developments of high resolution optical imaging system, manufacturing of lenses with ultra large aperture becomes increasingly difficult for traditional optical telescope system. By modulating the true thermal light from each point of object into a spatial pseudo-thermal light with a spatial random phase modulator, we propose a lensless Wiener-Khinchin telescope based on high-order spatial autocorrelation of light field. It can acquire the information of object from the second-order spatial intensity autocorrelation of light field in a single-shot measurement. The field of view and resolution of lensless Wiener-Khinchin telescope are quantitatively characterized and analyzed comparing with experimental results. As a new lensless imaging method, lensless Wiener-Khinchin telescope can be applied in many applications such as astronomical observations and X-rays imaging. © 2019 Optical Society of America under the terms of the OSA Open Access Publishing Agreement

**OCIS codes:** (110.0110) Imaging systems; (110.1758) Computational imaging; (110.6150) Speckle imaging; (350.1260) Astronomical optics; (290.5825) Scattering theory.

<http://dx.doi.org/10.1364/optica.XX.XXXXXX>

## 1. INTRODUCTION

Resolution is always an important issue in various fields of scientific researches and engineering applications, including microscopy, astronomy, and photography. Many great work and discussions of resolution have been made by a lot of researchers[1, 2]. From these work, we know that the operating wavelength  $\lambda$  and the aperture  $D$  of imaging system are two key parameters for optical resolution[1, 2]. Normally, the resolution is proportional to  $\lambda/D$ , therefore, in order to achieve higher resolution, shorter wavelength and larger aperture is required. With the increase of optical aperture, manufacturing of a traditional monolithic aperture optical telescope system has become increasingly difficult. In order to break through the limitation of conventional monolithic aperture lens, deployable segmented imaging[3], membrane imaging[4], diffractive imaging[5, 6], lensless imaging[7–15], Fourier-transform telescope[16, 17], and interferometric synthetic aperture imaging[18, 19] are proposed respectively. In these imaging methods, lensless imaging as a computational imaging method is an appropriate scheme for more and more large (decameters and hectometers) aperture of imaging system.

In the last few years, lensless point-scanning imaging[7], coherent diffractive imaging[9, 10, 20, 21], lensless compressive sensing imaging[8, 13, 14, 22], and lensless ghost imaging[11, 12, 23] etc. have obtained considerable development. Different from conventional imaging, ghost imaging (also called as correlated imaging)[24–27] obtain the information of object through second or higher order intensity mutual-correlation of light fields with and without targets, which open new avenues of lensless imaging from the perspective of the imaging mechanism.

According to illumination source, ghost imaging with thermal light can be classified to two categories: ghost imaging with pseudo-thermal light and ghost imaging with true thermal light or sunlight[28]. Ghost imaging with true thermal light or sunlight has been demonstrated by detecting the temporal fluctuation of light field, and imaging information was obtained by the second-order intensity correlation of light fields with and without targets in time domain[12, 29]. This scheme requires that the time resolution of detector is close to or less than the coherence time of light field  $\tau = \frac{\lambda^2/\Delta\lambda}{c} \propto \frac{1}{\lambda}$  ( $\lambda$  is the center wavelength,  $\Delta\lambda$  is the wavelength bandwidth,  $c$  is the speed of light) which can be as short as femtosecond[12, 28, 30]. In another

scheme for ghost imaging with true thermal light or sunlight, the true thermal light or sunlight is modulated into a spatially fluctuating pseudo-thermal light field by utilizing a spatial random phase modulator, and the object is obtained by the second-order intensity mutual-correlation of light fields with and without targets in spatial domain[28]. Therefore, the information of an object can be acquired in a single-shot measurement, and high time resolution isn't required in this scheme.

In this paper, we propose a lensless Wiener-Khinchin telescope based on high-order spatial autocorrelation of light field (conveniently called 'lensless Wiener-Khinchin telescope'). By modulating the true thermal light from each point of the object into a spatial pseudo-thermal light with a spatial random phase modulator, it obtains the information of an object from the second-order spatial intensity fluctuation autocorrelation of light field. Lensless Wiener-Khinchin telescope expands the ghost imaging technology based on mutual-correlation of light fields with and without targets to autocorrelation of light field with targets. As a new lensless imaging scheme, it will open a convenient and feasible way for applications in astronomical observation, remote sensing, and X-rays imaging.

## 2. METHOD

### A. System Schematic

The schematic of a lensless Wiener-Khinchin telescope (Figure 1) consists of a spatial random phase modulator and a charge-coupled device (CCD) detector. CCD detector is fixed behind the spatial random phase modulator, which detects the intensity distribution of modulated light field. The object is illuminated by a true thermal light source.

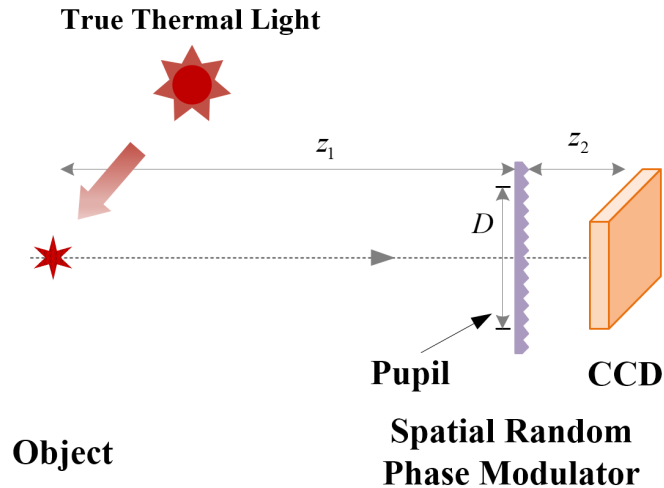


**Fig. 1.** Schematic of lensless Wiener-Khinchin telescope based on high-order spatial autocorrelation of light field. It consists of a spatial random phase modulator and a CCD detector. CCD detector is fixed behind the spatial random phase modulator, which detects the intensity distribution of modulated light field. The illumination source is a true thermal light source.

According to the incoherent imaging theory[31], the measured intensity distribution on the CCD detector is

$$I_t(r) = \int_{-\infty}^{\infty} I_0(r_0)h_I(r;r_0)dr_0 \quad , \quad (1)$$

where  $I_0(r)$  is the intensity distribution in the object plane,  $h_I(r_0)$  is the incoherent intensity impulse response function,  $r$  is the coordinate in CCD detector,  $r_0$  is the coordinate in the object plane. Since the target of a telescope is very small compared with the imaging distance, the space translation invariance (also known as memory effect[32, 33]) of system is satisfied, so we have

$$I_t(r) = \int_{-\infty}^{\infty} I_0(r_0)h_I(r;r_0)dr_0 = \{I_0(r_0) \otimes h_I(r_0)\}_{r_0 \rightarrow -\frac{z_1}{z_2}r} \quad , \quad (2)$$

where  $\otimes$  denotes the operation of convolution.

And the second-order spatial intensity autocorrelation function of the measured intensity distribution is

$$G_t^{(2)}(r + \Delta r, r) = \langle E_t^*(r + \Delta r) E_t^*(r) E_t(r) E_t(r + \Delta r) \rangle \\ = \iint_{-\infty}^{\infty} G_h^{(2)}(r + \Delta r, r'_0; r, r_0) I_0(r_0) I_0(r'_0) dr_0 dr'_0 \quad , \quad (3)$$

where

$$G_h^{(2)}(r + \Delta r, r'_0; r, r_0) = \langle h_E^*(r + \Delta r; r'_0) h_E^*(r; r_0) h_E(r; r_0) h_E(r + \Delta r; r'_0) \rangle \quad (4)$$

is the second-order correlation function of the incoherent intensity impulse response distribution, and  $h_E(r; r_0)$  is the point-spread function (PSF),  $\langle \dots \rangle$  is the ensemble average over spatial domain. Assuming that the point-spread function  $h_E(r; r_0)$  through the spatial random phase modulator obeys the complex circular Gaussian distribution in spatial domain[28],  $G_h^{(2)}(r + \Delta r, r'_0; r, r_0)$  can be written as

$$G_h^{(2)}(r + \Delta r, r'_0; r, r_0) \\ = \langle h_E^*(r + \Delta r; r'_0) h_E^*(r; r_0) h_E(r; r_0) h_E(r + \Delta r; r'_0) \rangle \\ = \langle h_E^*(r; r_0) h_E(r; r_0) \rangle \langle h_E^*(r + \Delta r; r'_0) h_E(r + \Delta r; r'_0) \rangle \\ + \langle h_E^*(r + \Delta r; r'_0) h_E(r; r_0) \rangle \langle h_E(r + \Delta r; r'_0) h_E^*(r; r_0) \rangle \\ = B [1 + g_h^{(2)}(r + \Delta r, r'_0; r, r_0)] \quad (5)$$

with  $B = \langle h_I(r; r_0) \rangle \langle h_I(r + \Delta r; r'_0) \rangle$ , and

$$g_h^{(2)}(r + \Delta r, r'_0; r, r_0) = \frac{|\langle h_E^*(r + \Delta r; r'_0) h_E(r; r_0) \rangle|^2}{\langle h_I(r; r_0) \rangle \langle h_I(r + \Delta r; r'_0) \rangle} \quad (6)$$

is defined as the normalized second-order correlation of the incoherent intensity impulse response distribution.

According to the Fresnel diffraction theorem[28], the PSF of lensless Wiener-Khinchin telescope is

$$h_E(r; r_0) = -\frac{1}{\lambda^2 z_1 z_2} \exp \left\{ \frac{j(r - r_0)^2}{\lambda(z_1 + z_2)} \right\} \\ \int_{-\infty}^{\infty} P(r_m) t(r_m) \exp \left\{ \frac{j\pi(z_1 + z_2)}{\lambda z_1 z_2} \left[ r_m - \frac{z_1 r + z_2 r_0}{z_1 + z_2} \right]^2 \right\} dr_m \quad (7)$$

where  $P(r_m)$  is the pupil function of the spatial random phase modulator,  $t(r_m) = \exp [j2\pi(n - 1)\eta(r_m)/\lambda]$  is the transmission function of spatial random phase modulator,  $\eta(r_m)$  is the height of spatial random phase modulator,  $n$  is the refractive index of spatial random phase modulator.

Substituting Eq. (7) into Eq. (6) yields

$$\begin{aligned}
& g_h^{(2)}(r + \Delta r, r'_0; r, r_0) \\
&= \frac{1}{B} \left| \iint_{-\infty}^{\infty} P(r_m) P^*(r_n) \langle t(r_m) t^*(r_n) \rangle \right. \\
& \exp \left\{ j \frac{\pi(z_1 + z_2)}{\lambda z_1 z_2} \left( r_m - \frac{z_1 r + z_2 r_0}{z_1 + z_2} \right)^2 \right\} \\
& \left. \exp \left\{ -j \frac{\pi(z_1 + z_2)}{\lambda z_1 z_2} \left( r_n - \frac{z_1(r + \Delta r) + z_2(r_0 + \Delta r_0)}{z_1 + z_2} \right)^2 \right\} dr_m dr_n \right|^2 \quad (8)
\end{aligned}$$

with  $\Delta r_0 = r'_0 - r_0$ .

In order to simplify the calculation, we make a convenient mathematical assumption about the form of the height ensemble average of the spatial random phase modulator  $R_\eta(r_m, r_n)$ [28], namely let

$$\begin{aligned}
R_\eta(r_m, r_n) &= \langle \eta(r_m) \eta(r_n) \rangle \\
&= \omega^2 \exp \left\{ -\left( \frac{r_m - r_n}{\zeta} \right)^2 \right\} = R_\eta(\Delta r_m), \quad \Delta r_m = r_m - r_n, \quad (9)
\end{aligned}$$

where  $\eta(r_h)$  is the height of spatial random phase modulator at  $r_h$ ,  $\omega$  and  $\zeta$  are respectively the height standard deviation and transverse correlation length of the spatial random phase modulator. Thus, we obtain (full derivation in Supplementary Materials)

$$\begin{aligned}
& g_h^{(2)}(r + \Delta r, r'_0; r, r_0) \\
& \approx \left| \left\{ \exp \left\{ -2 \left[ \frac{2\pi(n-1)}{\lambda} \right]^2 \left[ \omega^2 - R_\eta \left( \frac{2\lambda z_1 z_2}{z_1 + z_2} \nu \right) \right] \right\} \right. \right. \\
& \left. \left. \otimes \mathcal{F} \left\{ |P(\mu + \mu_0)|^2 \right\}_{\mu \rightarrow \nu} \right\} \frac{z_1 \Delta r + z_2 \Delta r_0}{2\lambda z_1 z_2} \right|^2 \quad (10) \\
& = g_h^{(2)} \left( \frac{z_1 \Delta r + z_2 \Delta r_0}{2\lambda z_1 z_2} \right),
\end{aligned}$$

where

$$\mu_0 = \frac{z_1(2r + \Delta r) + z_2(2r_0 + \Delta r_0)}{2(z_1 + z_2)} \quad (11)$$

Take Eqs. (5)(10) into Eq. (3), we have

$$\begin{aligned}
& G_i^{(2)}(r + \Delta r, r) \\
& \approx B \left\{ \left[ 1 + g_h^{(2)} \left( \frac{\Delta r_0}{2\lambda z_1} \right) \right] \otimes [I_0(\Delta r_0) \star I_0(\Delta r_0)] \right\}_{f_{r_0 \rightarrow \Delta r_0}} \left| \right|_{-\frac{z_1}{z_2} \Delta r} \quad (12)
\end{aligned}$$

where

$$I_0(\Delta r_0) \star I_0(\Delta r_0) = \int_{-\infty}^{\infty} I_0(r_0) I_0(r_0 + \Delta r_0) dr_0 \quad (13)$$

and

$$\begin{aligned}
& g_h^{(2)} \left( \frac{\Delta r_0}{2\lambda z_1} \right) \\
&= \left| \left\{ \exp \left\{ -2 \left[ \frac{2\pi(n-1)}{\lambda} \right]^2 \left[ \omega^2 - R_\eta \left( \frac{2\lambda z_1 z_2}{z_1 + z_2} \nu \right) \right] \right\} \right. \right. \\
& \left. \left. \otimes \mathcal{F} \left\{ |P(\mu + \mu_0)|^2 \right\}_{\mu \rightarrow \nu} \right\} \frac{\Delta r_0}{2\lambda z_1} \right|^2 \quad (14)
\end{aligned}$$

with  $\star$  denotes the operation of autocorrelation.

According to the Wiener-Khinchin theorem[34], we have

$$\begin{aligned}
& I_0(\Delta r_0) \star I_0(\Delta r_0) \\
&= \int_{-\infty}^{\infty} I_0(r_0) I_0(r_0 + \Delta r_0) dr_0 \\
&= \mathcal{F}^{-1} \left\{ \left| \mathcal{F} \{ I_0(r_0) \}_{r_0 \rightarrow f_{r_0}} \right|^2 \right\}_{f_{r_0 \rightarrow \Delta r_0}} \quad (15)
\end{aligned}$$

Substituting Eq. (15) into Eq. (12), we obtain

$$\begin{aligned}
& G_i^{(2)}(r + \Delta r, r) \\
& \propto \left\{ \left[ 1 + g_h^{(2)} \left( \frac{\Delta r_0}{2\lambda z_1} \right) \right] \otimes \mathcal{F}^{-1} \left\{ \left| \mathcal{F} \{ I_0(r_0) \}_{r_0 \rightarrow f_{r_0}} \right|^2 \right\}_{f_{r_0 \rightarrow \Delta r_0}} \right\}_{-\frac{z_1}{z_2} \Delta r} \quad (16)
\end{aligned}$$

Eq.(16) indicates that the Fourier transform amplitude of intensity distribution  $I_0(r_0)$  in the object plane  $\left| \mathcal{F} \{ I_0(r_0) \}_{r_0 \rightarrow f_{r_0}} \right|$  can be separated from the second-order autocorrelation function of the measured intensity distribution  $G_i^{(2)}(r + \Delta r, r)$ , and the resolution is determined by the normalized second-order correlation of the incoherent intensity impulse response distribution  $g_h^{(2)} \left( \frac{\Delta r_0}{2\lambda z_1} \right)$ . In detail, we take the following sign:

$$\begin{aligned}
Y &= \left| \mathcal{F} \{ I_0(r_0) \}_{r_0 \rightarrow f_{r_0}} \right|^2 \\
X &= I_0(r_0) \quad (17)
\end{aligned}$$

For Eq.(15), we have

$$y_k = x^* a_k^* a_k x = x^* A_k x = \text{Tr}(A_k X), \quad (18)$$

with  $a_k$  denoting the measurement vectors of digital Fourier transform,  $A_k = a_k^* a_k$ , and  $X = x x^*$ . Therefore, the object  $I_0(r_0)$  can be reconstructed by utilizing phase retrieval algorithms[35–45]. For the incoherent imaging,  $x$  is an amplitude object, which much improves the reconstruction quality with this constraint[46].

### 3. SYSTEM ANALYSIS

Field of view(FoV) and resolution are the key parameters of imaging system, so we briefly analyze FoV and optical resolution of the Wiener-Khinchin telescope.

#### A. Field of View

According to the imaging model and theoretical derivation of lensless Wiener-Khinchin telescope based on high-order spatial autocorrelation of light field, FoV is limited by the memory effect range of the imaging system[32, 33, 47, 48]. In consideration of spatial random phase modulator with height distribution, the normalized intensity correlation function between different incident angles without transverse translation is given by (full derivation in Supplementary Material)

$$\begin{aligned}
& g_\theta^{(2)}(\Delta \theta) = \exp \left\{ - \left[ \frac{2\pi\omega}{\lambda} \left( \sqrt{n^2 - \sin^2(\Delta \theta_i)} - n \right) \right]^2 \right\} \\
& \approx \exp \left\{ - \left( \frac{\pi n \omega}{\lambda} \sin^2(\Delta \theta) \right)^2 \right\} \quad (19)
\end{aligned}$$

where  $\Delta\theta$  is the variation of incident angle,  $\omega$  is the height standard deviation of the spatial random phase modulator. According to Eq. (19), the full width at half maximum (FWHM) of  $g_{\theta}^{(2)}(\Delta\theta)$  is proportional to  $\frac{\lambda}{\omega}$ , therefore, FoV of the lensless Wiener-Khinchin telescope increases with  $\frac{\lambda}{\omega}$ .

On the other hand, Eq. (12) and the Fourier transform&inverse Fourier transform in Eq.(15) lead to a limitation of FoV of the lensless Wiener-Khinchin telescope

$$FoV < \frac{S}{z_2} \quad (20)$$

with  $S$  denoting the detecting area of the CCD detector. This equation indicates that FoV of reconstructed image is also limited by the detecting area of the CCD detector. In order to obtain a large FoV, the detecting area of the CCD detector in the lensless Wiener-Khinchin telescope is selected much larger than  $\frac{\lambda z_2}{\omega}$  in Eq. (19).

## B. Optical Resolution

On the base of Eq.(12), optical resolution is determined by the normalized second-order correlation of the incoherent intensity impulse response distribution  $g_h^{(2)}\left(\frac{\Delta r_0}{2\lambda z_1}\right)$ , which is precisely expressed in Eq.(14). It shows that optical resolution is not only effected by the height distribution and the pupil function of the spatial random phase modulator, but also the distance between the spatial random phase modulator and the CCD detector.

According to the operation of convolution in  $g_h^{(2)}\left(\frac{\Delta r_0}{2\lambda z_1}\right)$ , we discuss two cases separately to simplify the analysis in the following contents.

### Case 1:

When the FWHM of  $\exp\left\{-2\left[\frac{2\pi(n-1)}{\lambda}\right]^2\left[\omega^2 - R_{\eta}\left(\frac{2\lambda z_1 z_2}{z_1 + z_2}\right)\right]\right\}$  is much larger than the FWHM of  $\mathcal{F}\left\{|P(\mu + \mu_0)|^2\right\}_{\mu \rightarrow \nu}$ , we have

$$\begin{aligned} g_h^{(2)}\left(\frac{\Delta r_0}{2\lambda z_1}\right) &\approx \left| \mathcal{F}\left\{|P(\mu + \mu_0)|^2\right\}_{\mu \rightarrow \frac{\Delta r_0}{2\lambda z_1}} \right|^2 \\ &= \left| \mathcal{F}\left\{|P(\mu)|^2\right\}_{\mu \rightarrow \frac{\Delta r_0}{2\lambda z_1}} \right|^2 \end{aligned} \quad (21)$$

For a circle aperture of the spatial random phase modulator,  $P(\mu) = \text{circ}\left(\frac{\mu}{D}\right)$ , and this leads to

$$g_h^{(2)}\left(\frac{\Delta r_0}{2\lambda z_1}\right) \propto \left[ \frac{J_1\left(\frac{2\pi D \Delta r_0}{z_1 \lambda}\right)}{\frac{2\pi D \Delta r_0}{z_1 \lambda}} \right]^2 \quad (22)$$

Under this condition, FWHM of  $g_h^{(2)}\left(\frac{\Delta r_0}{2\lambda z_1}\right)$  is proportional to  $\lambda z_1/D$ . In words, optical resolution capability of lensless Wiener-Khinchin telescope grows linearly with the aperture of the spatial random phase modulator, and is independent on the detecting distance  $z_2$ .

### Case 2:

When the FWHM of  $\exp\left\{-2\left[\frac{2\pi(n-1)}{\lambda}\right]^2\left[\omega^2 - R_{\eta}\left(\frac{2\lambda z_1 z_2}{z_1 + z_2}\right)\right]\right\}$  is much less than the FWHM of  $\mathcal{F}\left\{|P(\mu + \mu_0)|^2\right\}_{\mu \rightarrow \nu}$ , therefore,

$$\begin{aligned} &g_h^{(2)}\left(\frac{\Delta r_0}{2\lambda z_1}\right) \\ &\approx \exp\left\{-4\left[\frac{2\pi(n-1)\omega}{\lambda}\right]^2\left\{1 - \exp\left\{-\left[\frac{z_2 \Delta r_0}{(z_1 + z_2)\zeta}\right]^2\right\}\right\}\right\} \\ &\approx \exp\left\{-4\left[\frac{2\pi(n-1)\omega z_2 \Delta r_0}{\lambda(z_1 + z_2)\zeta}\right]^2\right\}, \end{aligned} \quad (23)$$

where the first-order approximation  $\exp\left\{-\left[\frac{z_2 \Delta r_0}{(z_1 + z_2)\zeta}\right]^2\right\} \approx 1 - \left[\frac{z_2 \Delta r_0}{(z_1 + z_2)\zeta}\right]^2$ . Under this condition, the FWHM of  $g_h^{(2)}\left(\frac{\Delta r_0}{2\lambda z_1}\right)$  is proportional to  $\left(1 + \frac{z_1}{z_2}\right)\frac{\lambda\zeta}{(n-1)\omega}$ . We see that the optical resolution grows with the detecting distance  $z_2$ , and gets better with  $\frac{\omega}{\zeta}$  increasing.

In terms of digital images, the construction of the image is also affected by the pixel size of CCD detector. Due to Eq. (12) and Fourier transform&inverse Fourier transform in Eq. (15), the pixel size of CCD detector is required by

$$P_{s_{detector}} < M \frac{z_2}{z_1} g_h^{(2)}\left(\frac{\Delta r_0}{2\lambda z_1}\right) \quad (24)$$

with  $M$  denoting the split number for discretization of optical resolution. For **Case 1**, according to Eq. (22), FWHM of  $g_h^{(2)}\left(\frac{\Delta r_0}{2\lambda z_1}\right)$  is proportional to  $\lambda z_1/D$ , and taking this result into Eq. (24), the pixel size of CCD detector is required smaller than  $M\frac{\lambda z_2}{D}$ . Similarly, for **Case 2**, the pixel size of CCD detector is required smaller than  $M\frac{\lambda\zeta}{(n-1)\omega}$  with  $z_1 \ll z_2$  in a telescope scheme.

## 4. EXPERIMENTAL RESULTS

The experimental setup of lensless Wiener-Khinchin telescope (shown in Figure 2) consists of a spatial random phase modulator (Thorlabs, DGVU10-220 - Ø1" UV Fused Silica Ground Glass Diffuser, refractive index  $n = 1.46$ ) with height standard deviation  $\omega = 1.1\mu\text{m}$  and transverse correlation length  $\zeta = 44\mu\text{m}$ , a microscope objective with a magnification factor  $\beta = 10$  and a numerical aperture  $N.A. = 0.25$  which magnifies the measured intensity distribution, and a CCD detector (APGCCD) with a pixel size  $13\mu\text{m} \times 13\mu\text{m}$ , which records the magnified intensity distribution. Object is illuminated by a true thermal light source (hydrogen lamp). We have to point out that the microscope is only used to amplify the intensity distribution on the speckle plane to match the pixel size of the CCD detector, and is not necessary in some experimental conditions.

In order to analyze optical resolution of lensless Wiener-Khinchin telescope, a double slit with a  $180\mu\text{m}$  joint spacing (shown in Figure 3(a)) was selected. Although lensless

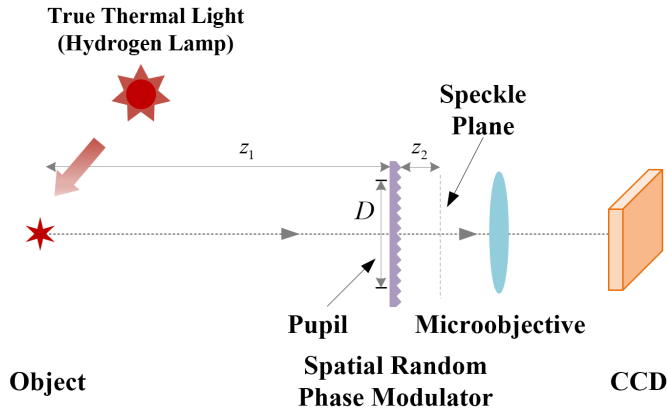


**Fig. 2.** The experimental setup of lensless Wiener-Khinchin telescope. It consists of a spatial random phase modulation, a micro-objective, and a CCD detector. The target is illuminated by a true thermal light source (hydrogen lamp).

Wiener-Khinchin telescope obtains the ensemble average information of target in spatial domain, where the temporal coherence of light source isn't strictly required, it still suffers from the chromatic aberrations due to the dispersion of spatial random phase modulator during propagation. Therefore, the operating wavelength bandwidth is also explored in the experiment. We choose different operating wavelength bandwidths:  $\lambda = 532nm$  with bandwidths of  $3nm$  and  $10nm$ ,  $\lambda = 550nm$  with bandwidths of  $10nm$ ,  $25nm$ , and  $50nm$  in experiment, while imaging distance  $z_1 = 0.15m$ , detecting distance between the spatial random phase modulator and detected speckle plane  $z_2 = 12mm$ , and the aperture of the spatial random phase modulator  $D = 8mm$  are fixed. Figure 3(b-f) shows the reconstruction results of the double slit with different operating wavelength by applying the same phase retrieval algorithm respectively[38]. The experimental results demonstrate that lensless Wiener-Khinchin telescope can partly tolerate the dispersion due to wider wavelength bandwidth.  $\lambda = 532nm$  with a bandwidth of  $10nm$  is identified as the operating wavelength of lensless Wiener-Khinchin telescope in subsequent experiments.

According to Eq.(21), optical resolution is affected by the aperture of spatial random phase modulator. Therefore, we change the aperture of the spatial random phase modulator to observe the change of optical resolution. Five different apertures ( $D = 4mm, 4.5mm, 5mm, 6mm, 8mm$ ) are set accordingly, and the reconstructed images are shown in Figure 4(b-f) respectively, while  $z_1 = 1.1m$  and  $z_2 = 60mm$  are fixed. These parameters are selected in accordance with Case 1, and according to Eq.(23), the corresponding optical resolution with different apertures of the spatial random phase modulator is shown in Figure 5, where the FWHMs for  $D = 4.5mm$ ,  $D = 5mm$ ,  $D = 5.5mm$ ,  $D = 6mm$  and  $D = 8mm$  are  $150\mu m$ ,  $134\mu m$ ,  $121\mu m$ ,  $100\mu m$  and  $75\mu m$ , respectively. Figure 6 shows the optical resolution comparison between theoretical result and experimental result with  $D = 5mm$ , where the red line is a cross-section curve of Figure 4(d). The experimental results shows that double slit can be distinguished with aperture  $D = 5mm$ , and optical resolution will be higher with wider aperture of the spatial random phase modulator, which verifies the previous analysis for Eq.(23).

Optical resolution is also mainly affected by the distance between the spatial random phase modulator and the detected

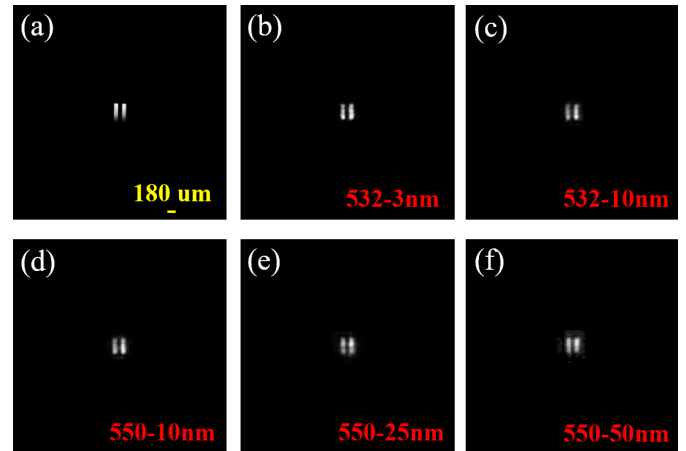


**Fig. 3.** Double slit experimental result with different operating wavelength bandwidths. (a) Reference image: the distance of the double slit is  $180\mu m$ . Reconstructed images for operating wavelength: (b)  $\lambda = 532nm$  with a  $3nm$  bandwidth, (c)  $\lambda = 532nm$  with a  $10nm$  bandwidth, (d)  $\lambda = 550nm$  with a  $10nm$  bandwidth, (e)  $\lambda = 550nm$  with a  $25nm$  bandwidth, (f)  $\lambda = 550nm$  with a  $50nm$  bandwidth. Imaging distance  $z_1 = 0.15m$ , detecting distance  $z_2 = 12mm$ , and the aperture of the spatial random phase modulator  $D = 8mm$ .

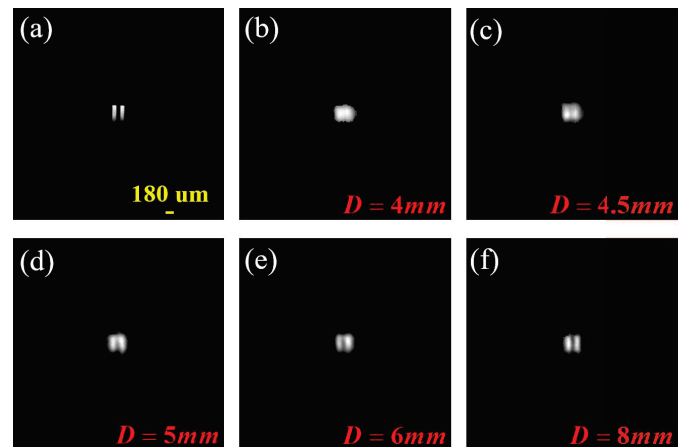


**Fig. 4.** Double slit experimental result with different apertures of spatial random phase modulator. (a) Reference image: the distance of double slit is  $180\mu m$ . Reconstructed images with five apertures of spatial random phase modulator: (b)  $D = 4mm$ , (c)  $D = 4.5mm$ , (d)  $D = 5mm$ , (e)  $D = 6mm$ , (f)  $D = 8mm$ . Imaging distance  $z_1 = 1.1m$ , detecting distance  $z_2 = 60mm$ .



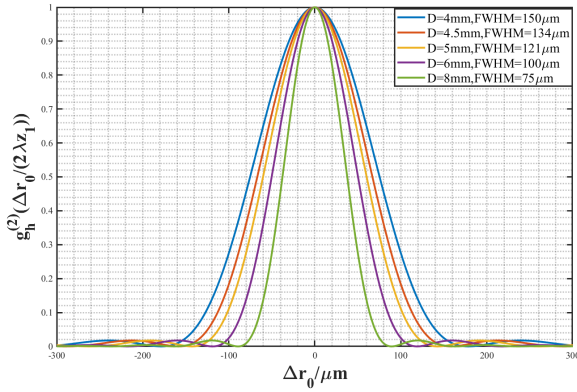


**Fig. 5.** Optical resolution with five different apertures of the spatial random phase modulator.

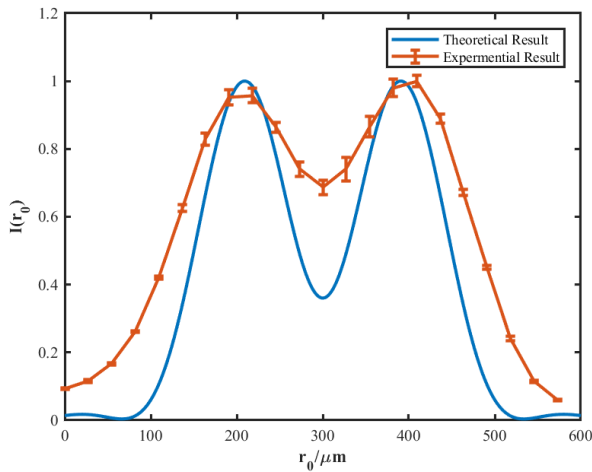


**Fig. 6.** The optical resolution comparison between theoretical result and experimental result with aperture  $D = 5mm$ . The red line is a cross-section curve of Figure 4(d)

speckle plane according to Eq. (23). Five different detecting distances ( $z_2 = 4mm, 6mm, 8mm, 10mm, 12mm$ ) are set, and the reconstructed images are shown in Figure 7(b-f) respectively, while the imaging distance  $z_1 = 0.3m$  and the aperture of the spatial random phase modulator  $D = 8mm$  are fixed. These parameters are selected in accordance with Case 2, and according to Eq.(23), the corresponding optical resolution with different distances is shown in 8, where the FWHMs for  $z_2 = 4mm, z_2 = 6mm, z_2 = 8mm, z_2 = 10mm$  and  $z_2 = 12mm$  are  $313\mu m, 211\mu m, 160\mu m, 129\mu m$  and  $108\mu m$ , respectively. Figure 9 shows the optical resolution comparison between theoretical result and experimental result with detecting distance  $z_2 = 8mm$ , where the red line is a cross-section curve of Figure 7(d). The experimental result shows that the double slit can be distinguished with detecting distance  $z_2 = 8mm$ , and optical resolution will get better with the increased detecting distance between the spatial random phase modulator and detected speckle plane, which is consistent with analysis for Eq.(23).

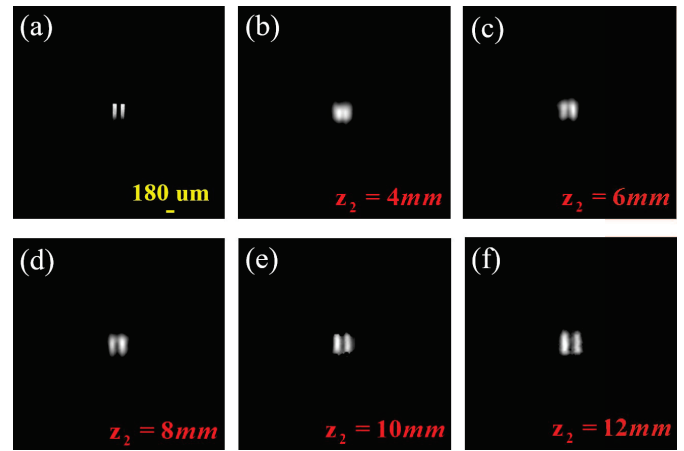


**Fig. 7.** Double slit experimental result with different distances between the spatial random phase modulator and detected speckle plane. (a) Reference image: the distance of double slit is  $180\mu m$ . Reconstructed images with five detecting distances between the spatial random phase modulator and detected speckle plane: (b)  $z_2 = 4mm$ , (c)  $z_2 = 6mm$ , (d)  $z_2 = 8mm$ , (e)  $z_2 = 10mm$ , (f)  $z_2 = 12mm$ . Imaging distance  $z_1 = 0.3m$ , the aperture of spatial random phase modulator  $D = 8mm$ .

For a telescope, the imaging distance  $z_1$  is nearly infinitely far away, which means  $z_1 \gg z_2$ , so the resolution  $g_h^{(2)}\left(\frac{\Delta r_0}{2\lambda z_1}\right)$  in Eq. (12) is approximated to

$$g_h^{(2)}\left(\frac{\Delta r_0}{2\lambda z_1}\right) \propto \left| \left\{ \exp \left\{ -2 \left[ \frac{2\pi(n-1)}{\lambda} \right]^2 \left[ \omega^2 - R_\eta(2\lambda z_2 \nu) \right] \right\} \otimes \mathcal{F} \left\{ |P(\mu)|^2 \right\}_{\mu \rightarrow \nu} \right\} \frac{\Delta r_0}{2\lambda z_1} \right|^2 \quad (25)$$

Therefore, we take an object ‘GI’ (shown in Figure 10(a)) in the focal plane of an optical lens to experimentally simulate the target placed infinitely far away. The target can be well reconstructed, which is shown in Figure 10(b).

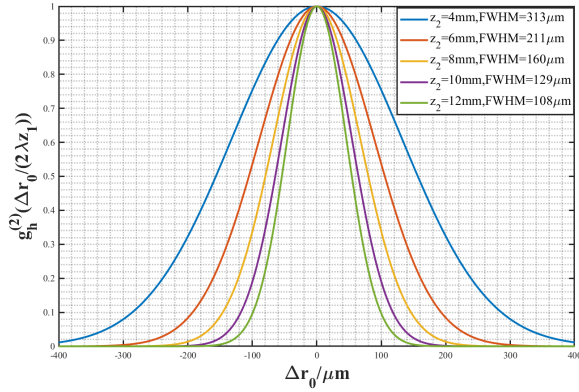


**Fig. 8.** Optical resolution with five different distances between the spatial random phase modulator and detected speckle plane. The FWHMs for  $z_2 = 4mm$ ,  $z_2 = 6mm$ ,  $z_2 = 8mm$ ,  $z_2 = 10mm$  and  $z_2 = 4mm$  are  $313\mu m$ ,  $211\mu m$ ,  $160\mu m$ ,  $129\mu m$  and  $108\mu m$ , respectively.

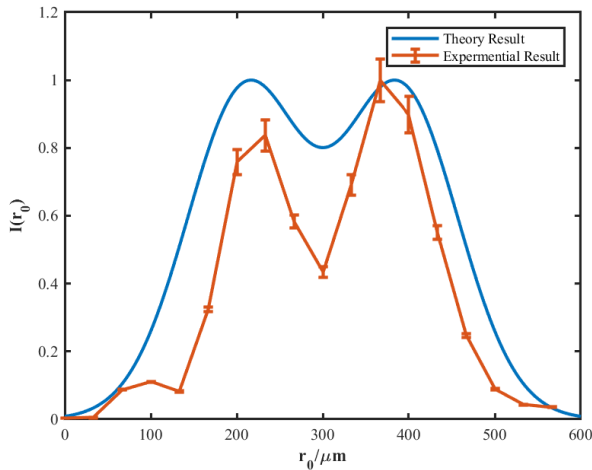


**Fig. 9.** The optical resolution comparison between theoretical result and experimental result with  $z_2 = 8mm$ . The red line is a cross-section curve of Figure 7(d).

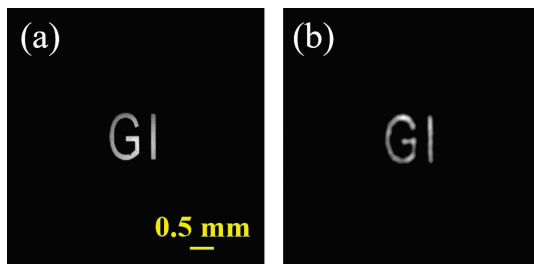


**Fig. 10.** An object 'GI' is put in the focal plane of an optical lens to experimentally simulate the target placed infinitely far away. (a) Reference image, (b) reconstructed image.

In order to verify the imaging capability of lensless Wiener-Khinchin telescope, images of two targets (' $\pi$ ' and 'panda') are shown in Figure 11, which are still illuminated by the true thermal light (hydrogen lamp). Different parameters are selected for the two targets. For the ' $\pi$ ',  $z_1 = 0.5m$ , the distance between the spatial random phase modulator and detected speckle plane  $z_2$  is  $2mm$ , and for the 'panda',  $z_1 = 1.5m$ , the distance  $z_2$  is  $3mm$ . The reconstructed images of ' $\pi$ ' and 'panda' are shown in Figure 12 respectively. The experimental results in Figure 12 demonstrate the imaging capability of the lensless Wiener-Khinchin telescope for natural targets.

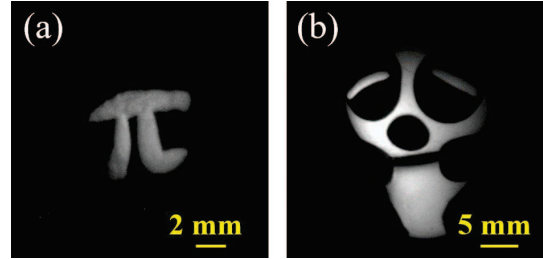


**Fig. 11.** Reference images of (a) ' $\pi$ ' and (b) 'panda'.

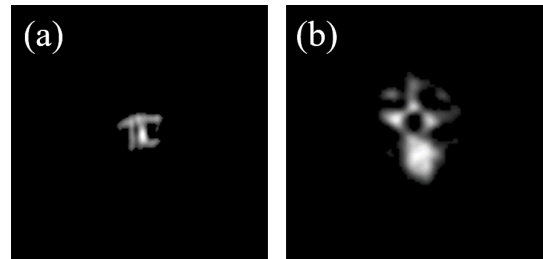


**Fig. 12.** Reconstructed images of (a) ' $\pi$ ' and (b) 'panda'. For the ' $\pi$ ',  $z_1 = 0.5m$ , the distance between the spatial random phase modulator and detected speckle plane  $z_2$  is  $2mm$ . For the 'panda',  $z_1 = 1.5m$ , the detecting distance  $z_2$  is  $3mm$ .

## 5. CONCLUSION

In this paper, we have proposed and demonstrated a novel and simple optical imaging system: lensless Wiener-Khinchin telescope based on high-order spatial autocorrelation of light field. It modulates the true thermal light from each point of the object into a spatial pseudo-thermal light based on spatial random phase modulation, and acquired the information of the object from the second-order spatial intensity autocorrelation of light field in a single-shot measurement. The FoV and resolution of lensless Wiener-Khinchin telescope are quantitatively characterized, analyzed, and compared with experimental results in this paper. Comparing with lensless compressive sensing imaging[8, 13, 14, 22] and lensless ghost imaging[11, 12, 23], the measurement matrix and calibration process is not required in lensless Wiener-Khinchin telescope, while the FoV of lensless Wiener-Khinchin telescope is limited by the memory effect of system. Lensless Wiener-Khinchin telescope can be applied in many applications, such as the astronomical observation, remote sensing and X-rays imaging. Moreover, regarding the spatial random phase modulator as the scattering medium, the framework of lensless Wiener-Khinchin telescope may af-

ford a starting point for a quantitative description of scattering imaging[49–53].

## FUNDING INFORMATION

National Key Research and Development Program of China No.2017YFB0503303. Hi-Tech Research and Development Program of China under Grant Project No.2013AA122902 and No.2013AA122901.

## ACKNOWLEDGMENTS

The authors thank the research team of professor Guohai Situ for helpful discussions.

See [Supplement 1](#) for supporting content.

## REFERENCES

1. C. J. Sheppard, "Resolution and super-resolution," *Microw. Res. Tech.* (2017).
2. S. Baker and T. Kanade, "Limits on super-resolution and how to break them," *IEEE Transactions on Pattern Analysis Mach. Intell.* **24**, 1167–1183 (2002).
3. M. A. Greenhouse, "The JWST science instrument payload: mission context and status," in "UV/Optical/IR Space Telescopes and Instruments: Innovative Technologies and Concepts VII," H. A. MacEwen and J. B. Breckinridge, eds. (SPIE, 2015).
4. M. Angel, "Eight-inch f5 deformable magnetic-membrane mirror," in "Optomechanical Technologies for Astronomy," E. Atad-Etchedgui, J. Antebi, and D. Lemke, eds. (SPIE, 2006).
5. R. A. Hyde, "Eyeglass 1 very large aperture diffractive telescopes," *Appl. Opt.* **38**, 4198 (1999).
6. P. D. Atcheson, C. Stewart, J. Domber, K. Whiteaker, J. Cole, P. Spuhler, A. Seltzer, J. A. Britten, S. N. Dixit, B. Farmer, and L. Smith, "MOIRE: initial demonstration of a transmissive diffractive membrane optic for large lightweight optical telescopes," in "Space Telescopes and Instrumentation 2012: Optical, Infrared, and Millimeter Wave," M. C. Clampin, G. G. Fazio, H. A. MacEwen, and J. M. Oschmann, eds. (SPIE, 2012).
7. Y. Cui, S. Schuon, D. Chan, S. Thrun, and C. Theobalt, "3d shape scanning with a time-of-flight camera," in "2010 IEEE Computer Society Conference on Computer Vision and Pattern Recognition," (IEEE, 2010).
8. G. Huang, H. Jiang, K. Matthews, and P. Wilford, "Lensless imaging by compressive sensing," in "2013 IEEE International Conference on Image Processing," (IEEE, 2013).
9. J. Miao, P. Charalambous, J. Kirz, and D. Sayre, "Extending the methodology of x-ray crystallography to allow imaging of micrometre-sized non-crystalline specimens," *Nature*. **400**, 342–344 (1999).
10. H. N. Chapman and K. A. Nugent, "Coherent lensless x-ray imaging," *Nat. Photonics* **4**, 833–839 (2010).
11. H. Yu, R. Lu, S. Han, H. Xie, G. Du, T. Xiao, and D. Zhu, "Fourier-transform ghost imaging with hard x rays," *Phys. review letters* **117**, 113901 (2016).
12. X.-F. Liu, X.-H. Chen, X.-R. Yao, W.-K. Yu, G.-J. Zhai, and L.-A. Wu, "Lensless ghost imaging with sunlight," *Opt. letters* **39**, 2314–2317 (2014).
13. N. Antipa, G. Kuo, R. Heckel, B. Mildenhall, E. Bostan, R. Ng, and L. Waller, "DiffuserCam: lensless single-exposure 3d imaging," *Optica* **5**, 1 (2017).
14. A. Zomet and S. Nayar, "Lensless imaging with a controllable aperture," in "2006 IEEE Computer Society Conference on Computer Vision and Pattern Recognition - Volume 1 (CVPR'06)," (IEEE).
15. J. K. Adams, V. Boominathan, B. W. Avants, D. G. Vercosa, F. Ye, R. G. Baraniuk, J. T. Robinson, and A. Veeraraghavan, "Single-frame 3d fluorescence microscopy with ultraminature lensless FlatScope," *Sci. Adv.* **3**, e1701548 (2017).
16. T. A. Prince, G. J. Hurford, H. S. Hudson, and C. J. Crannell, "Gamma-ray and hard x-ray imaging of solar flares," *Sol. Phys.* **118**, 269–290 (1988).
17. T. Kosugi, K. Makishima, T. Murakami, T. Sakao, T. Dotani, M. Inada, K. Kai, S. Masuda, H. Nakajima, Y. Ogawara, M. Sawa, and K. Shibasaki, "The hard x-ray telescope (HXT) for the SOLAR-a mission," in "The Yohkoh (Solar-A) Mission," (Springer Netherlands, 1991), pp. 17–36.
18. A. B. Meinel, "Aperture synthesis using independent telescopes," *Appl. Opt.* **9**, 2501 (1970).
19. C. Fridlund, "Darwin-the infrared space interferometry mission," *Eur. Space Agency Special Publ. SP* (2000).
20. B. Abbey, L. W. Whitehead, H. M. Quiney, D. J. Vine, G. A. Cadenazzi, C. A. Henderson, K. A. Nugent, E. Balaur, C. T. Putkunz, A. G. Peele, G. J. Williams, and I. McNulty, "Lensless imaging using broadband x-ray sources," *Nat. Photonics* **5**, 420–424 (2011).
21. J. Miao, T. Ishikawa, I. K. Robinson, and M. M. Murnane, "Beyond crystallography: Diffractive imaging using coherent x-ray light sources," *Science* **348**, 530–535 (2015).
22. M. S. Asif, A. Ayremlou, A. Sankaranarayanan, A. Veeraraghavan, and R. G. Baraniuk, "FlatCam: Thin, lensless cameras using coded aperture and computation," *IEEE Transactions on Comput. Imaging* **3**, 384–397 (2017).
23. X.-H. Chen, Q. Liu, K.-H. Luo, and L.-A. Wu, "Lensless ghost imaging with true thermal light," *Opt. Lett.* **34**, 695 (2009).
24. A. Gatti, E. Brambilla, M. Bache, and L. A. Lugiato, "Ghost imaging with thermal light: comparing entanglement and classical correlation," *Phys. review letters* **93**, 093602 (2004).
25. J. Cheng and S. Han, "Incoherent coincidence imaging and its applicability in x-ray diffraction," *Phys. review letters* **92**, 093903 (2004).
26. J. H. Shapiro, "Computational ghost imaging," *Phys. Rev. A* **78**, 061802 (2008).
27. J. H. Shapiro and R. W. Boyd, "The physics of ghost imaging," *Quantum Inf. Process.* **11**, 949–993 (2012).
28. Z. Liu, S. Tan, J. Wu, E. Li, X. Shen, and S. Han, "Spectral camera based on ghost imaging via sparsity constraints," *Sci. reports* **6** (2016).
29. D. Zhang, Y.-H. Zhai, L.-A. Wu, and X.-H. Chen, "Correlated two-photon imaging with true thermal light," *Opt. letters* **30**, 2354–2356 (2005).
30. R. H. BROWN and R. TWISS, "The question of correlation between photons in coherent light rays," *Nature* **178**, 1447–1448 (1956).
31. J. W. Goodman, *Introduction to Fourier optics*, 154-160 (Roberts and Company Publishers, 2005).
32. S. Feng, C. Kane, P. A. Lee, and A. D. Stone, "Correlations and fluctuations of coherent wave transmission through disordered media," *Phys. Rev. Lett.* **61**, 834–837 (1988).



33. G. Osnabrugge, R. Horstmeyer, I. N. Papadopoulos, B. Judkewitz, and I. M. Vellekoop, "Generalized optical memory effect," *Optica* **4**, 886 (2017).
34. L. Cohen, "The generalization of the wiener-khinchin theorem," in "Proceedings of the 1998 IEEE International Conference on Acoustics, Speech and Signal Processing, ICASSP '98 (Cat. No.98CH36181)," (IEEE).
35. J. R. Fienup, "Reconstruction of an object from the modulus of its fourier transform," *Opt. letters* **3**, 27–29 (1978).
36. J. R. Fienup, "Phase retrieval algorithms: a comparison," *Appl. optics* **21**, 2758–2769 (1982).
37. E. J. Candès, T. Strohmer, and V. Voroninski, "PhaseLift: Exact and stable signal recovery from magnitude measurements via convex programming," *Commun. on Pure Appl. Math.* **66**, 1241–1274 (2012).
38. X. Liu, J. Wu, W. He, M. Liao, C. Zhang, and X. Peng, "Vulnerability to ciphertext-only attack of optical encryption scheme based on double random phase encoding," *Opt. Express* **23**, 18955 (2015).
39. E. J. Candès, X. Li, and M. Soltanolkotabi, "Phase retrieval from coded diffraction patterns," *Appl. Comput. Harmon. Analysis* **39**, 277–299 (2015).
40. Y. Chen and E. Candès, "Solving random quadratic systems of equations is nearly as easy as solving linear systems," in "Advances in Neural Information Processing Systems 28," C. Cortes, N. D. Lawrence, D. D. Lee, M. Sugiyama, and R. Garnett, eds. (Curran Associates, Inc., 2015), pp. 739–747.
41. Y. Shechtman, Y. C. Eldar, O. Cohen, H. N. Chapman, J. Miao, and M. Segev, "Phase retrieval with application to optical imaging: a contemporary overview," *IEEE signal processing magazine* **32**, 87–109 (2015).
42. E. J. Candès, Y. C. Eldar, T. Strohmer, and V. Voroninski, "Phase retrieval via matrix completion," *SIAM Rev.* **57**, 225–251 (2015).
43. E. J. Candès, X. Li, and M. Soltanolkotabi, "Phase retrieval via wirtinger flow: Theory and algorithms," *IEEE Transactions on Inf. Theory* **61**, 1985–2007 (2015).
44. E. J. Candès, X. Li, and M. Soltanolkotabi, "Phase retrieval from coded diffraction patterns," *Appl. Comput. Harmon. Analysis* **39**, 277–299 (2015).
45. K. Jaganathan, S. Oymak, and B. Hassibi, "Sparse phase retrieval: Uniqueness guarantees and recovery algorithms," *IEEE Transactions on Signal Process.* **65**, 2402–2410 (2017).
46. G. Ying, Q. Wei, X. Shen, and S. Han, "A two-step phase-retrieval method in fourier-transform ghost imaging," *Opt. Commun.* **281**, 5130–5132 (2008).
47. D. Léger, E. Mathieu, and J. C. Perrin, "Optical surface roughness determination using speckle correlation technique," *Appl. Opt.* **14**, 872 (1975).
48. B. Judkewitz, R. Horstmeyer, I. M. Vellekoop, I. N. Papadopoulos, and C. Yang, "Translation correlations in anisotropically scattering media," *Nat. Phys.* **11**, 684–689 (2015).
49. J. Bertolotti, E. G. van Putten, C. Blum, A. Lagendijk, W. L. Vos, and A. P. Mosk, "Non-invasive imaging through opaque scattering layers," *Nature*. **491**, 232–234 (2012).
50. O. Katz, E. Small, and Y. Silberberg, "Looking around corners and through thin turbid layers in real time with scattered incoherent light," *Nat. Photonics* **6**, 549–553 (2012).
51. O. Katz, P. Heidmann, M. Fink, and S. Gigan, "Non-invasive single-shot imaging through scattering layers and around corners via speckle correlations," *Nat. photonics* **8**, 784–790 (2014).
52. X. Yang, Y. Pu, and D. Psaltis, "Imaging blood cells through scattering biological tissue using speckle scanning microscopy," *Opt. Express* **22**, 3405 (2014).
53. H. Zhuang, H. He, X. Xie, and J. Zhou, "High speed color imaging through scattering media with a large field of view," *Sci. reports* **6** (2016).